Cement & Concrete Composites 35 (2013) 181–189

Contents lists available at SciVerse ScienceDirect

Cement & Concrete Composites

journal homepage: www.elsevier.com/locate/cemconcomp

Effect of inhibitors on the corrosion of galvanized steel and on mortar properties

I. Fayala [a,*], L. Dhouibi [b], X.R. Nóvoa [c], M. Ben Ouezdou [a]

[a] Laboratoire de Génie Civil, ENIT, BP 37 Le Belvédère, 1002 Tunis, Tunisia
[b] Unité de recherche Corrosion et Protection des Métalliques, ENIT, 1002 Tunis, Tunisia
[c] ENCOMAT group, E.T.S.E.I., Universidade de Vigo, 36310 Vigo, Spain

ARTICLE INFO

Article history:
Received 24 June 2012
Received in revised form 16 August 2012
Accepted 18 August 2012
Available online 30 August 2012

Keywords:
Galvanized steel
Mortar microstructure
Corrosion inhibitors
Impedance Spectroscopy
Differential Scanning Calorimetry
Chlorides exposure

ABSTRACT

This work evaluates two complementary protection methods for steel in concrete: galvanizing coating and corrosion inhibitors. The study was undertaken to evaluate the efficiency of using inhibitors (sodium nitrite, diethanolamine) to protect galvanized reinforcements embedded in mortar against corrosion, and their effect on the mortar properties before and after exposure to chloride environments. Accelerated corrosion tests were performed on mortar specimens by wet–dry exposure to sodium chloride solution. The electrochemical behavior of rebars was studied using Electrochemical Impedance Spectroscopy; the results showed that diethanolamine improves the level of protection of the reinforcement. The influence of inhibitor additions on mortar properties was considered by characterizing the pore structure using Mercury Intrusion Porosimetry and by assessing the dielectric properties of mortar employing Impedance Spectroscopy. The results revealed that inhibitors addition leads to microstructural changes. Differential Scanning Calorimetry was applied on mortar samples to elucidate the causes of the observed microstructural changes.

1. Introduction

Reinforcement corrosion is the most widespread damage mechanism to which reinforced concrete structures are subjected when they are exposed to aggressive environments. Annual expenditures to repair corrosion damage are huge. To address this problem, implementation of corrosion protection systems should be considered when there is a risk of reinforcement corrosion, especially in marine environments. Among the existing protection methods to improve the corrosion resistance, galvanized reinforcements have been increasingly used as a preventive measure to delay the corrosion process of the steel substrate in the presence of aggressive agents such as chloride ions [1–6]. Indeed, the chloride threshold value of zinc is higher than that of ordinary steel reinforcement bars, so galvanized reinforcement lengthens the service life of structures exposed to chlorides [7].

Several studies have established that hot dip galvanized coatings exposed to simulated concrete pore solution develop very stable corrosion products at the coating surface due to the formation of a passive protective film at the interface identified as hydrozincite [8]. Results published by different authors on galvanized steel performance revealed that zinc coating decreased the extent of corrosion in sodium chloride exposure compared to ordinary steel [9]. Others [10] investigated the performance of galvanized steel embedded in cracked concrete immersed in seawater and their studies showed the occurrence of pitting corrosion observed at the cracks [11]. Hence, the galvanized steel passivity is lost once chloride content in the concrete exceeds a threshold concentration which is reported to be 2% [4]. When reinforced mortar specimens were exposed to artificial sea water, galvanized reinforcements abandoned their passive state within a few months, after which, corrosion attacks the substrate, yielding a rapid failure of the reinforcement that might lead to severe damage and loss of safety of the structure. Thus, galvanizing seems to be insufficient for long-term durability.

Moreover, the use of galvanizing as protective method did not obtain wide acceptance in the past due to the coating reaction with the surrounding aqueous phase of the mortar, yielding a change in the bond performance of galvanized bars. Studies performed on this topic present controversial results. The bond loss is attributed, according to some authors, to the hydrogen release around the galvanized reinforcement and according to others, to the possible changes in the mechanical characteristics of steel after galvanization [12]. The contradictory results obtained about bond performance of galvanized steel have been attributed to the use of different types of tests, different cements, and the different ages of the tested specimens [13].

Some researchers tried to prevent hydrogen gas evolution by applying conversion pre-treatments [14–17]. On the other hand, several researchers deal with the reinforcement corrosion problem by using corrosion inhibitors in the aim to inhibit the onset of chloride-induced corrosion of concrete reinforcement. Two issues need

* Corresponding author. Tel./fax: +216 71875726.
E-mail address: fayala_ines@yahoo.fr (I. Fayala).

0958-9465/$ - see front matter © 2012 Elsevier Ltd. All rights reserved.
http://dx.doi.org/10.1016/j.cemconcomp.2012.08.014

to be addressed in the use of corrosion inhibitors. First and foremost is the efficiency of inhibiting action which is the most obvious concern, and second, but of no lesser importance, is the influence of this inhibitor on concrete properties. According to some researchers [18] "an inhibitor adequate to control or to prevent corrosion of reinforcing steel must be a suitable chemical admixture, which when added to concrete in the correct proportions, should be able to stop or delay the reinforcement corrosion without adverse effects in the mechanical and physical–chemical properties of concrete".

Many researchers have been interested in the effect of inhibitors on concrete properties [19–21]. Some authors report that organic inhibitors help to decrease the chloride content in concrete and to promote a decrease on the chloride ion diffusion [19]. Unfortunately, none of these two preventive techniques are free of shortcomings and present some lacunae. Therefore, the use of additional protective measures becomes necessary to protect galvanized reinforcement bars embedded in concrete structures against corrosion in presence of high chloride concentration. For this reason, this study uses two complementary protection methods to improve the corrosion resistance of steel reinforcement in concrete exposed to marine-type environments: galvanized coating and corrosion inhibitors.

The objective of this work is to determine the effects of inhibitor additions (sodium nitrite and diethanolamine) on the corrosion resistance of galvanized reinforcing bars and on the mortar properties. A wet–dry cyclic test, which simulates marine environments, has been used to evaluate the corrosion behavior of galvanized steel. Those effects are evaluated in terms of polarization resistance for the galvanized reinforced specimens and pore microstructure and dielectric properties of mortar samples (permittivity and resistivity).

2. Specimens preparation and materials

Mortar samples were prepared using Portland cement CEM II/A-L 32.5 N. The chemical composition of the cement used is depicted in Table 1.

The sand employed was normalized type, and cement to sand ratio 0.33 was employed. Distilled water was used as mixing water with a water-to-cement (w:c) ratio equal to 0.6 in the purpose to have porous mortar and to accelerate the corrosion process. The corrosion inhibitors considered in this study were sodium nitrite (SN) and diethanolamine (DEA), used as preventive inhibitors. They were added to the water, during the mixing phase, in the concentration of 2% per weight of cement for SN and in the concentration of 3.5 L/m^3 of mortar for DEA. Smooth ordinary carbon steel rebars of 6 mm diameter and 12 cm length were used. Galvanized steel rebars were produced by hot dip galvanizing process which consists in dipping the ordinary carbon steel in molten zinc (450 °C). Specimens of (40 × 40 × 160 mm) were made by casting the mortar in prismatic molds. After 24 h, the specimens were demoulded and cured for 28 days in distilled water to ovoid any contamination. Reinforced specimens were also manufactured by embedding a galvanized rebar in the in the center of the specimen, with 1.7 cm mortar cover.

As can be seen in Table 2, some of these specimens (lot no. 2) were submitted, after the curing period, to alternate wetting and drying in sodium chloride solution in order to accelerate chloride penetration. One cycle consists of 3 days immersion in 3% NaCl solution and 3 days drying in open atmosphere. The experimentation went on up to the 7th wet–dry cycle for unreinforced specimens and to the 12th cycle for reinforced specimens. Unreinforced specimens were cut into slices with 0.86 cm average thickness to be used in the experiment part. The tests were carried out on triplicate specimens and the average values reported.

Table 1
Chemical composition of the cement, according to the producer.

Oxydes	SiO_2	Al_2O_3	Fe_2O_3	CaO	MgO	SO_3	K_2O
Content (%)	17.38	3.86	3.22	60.75	1.26	2.41	0.74

Table 2
Mortar specimens tested.

Specimen type	Labels	Inhibitor content
Lot no. 1: specimens after 28 days of curing		
Control specimen	S1(C)	–
Specimen with $NaNO_2$	S1(SN)	2%
Specimen with DEA	S1(DEA)	3.5 L/m^3
Lot no. 2: specimens after 28 days of curing + 7 cycles of wet–dry exposure to 3% NaCl solution		
Control specimen	S2(C)	–
Reinforced control specimen	S2(C,GS)	–
Specimen with $NaNO_2$	S2(NS)	2%
Reinforced specimen with $NaNO_2$	S2(NS,GS)	2%
Specimen with DEA	S2(DEA)	3.5 L/m^3
Reinforced specimen with DEA	S2(DEA,GS)	3.5 L/m^3

The labels shown are those used in the figures.

3. Experimental results

3.1. Electrochemical behavior of galvanized rebars

3.1.1. Experimental method

Electrochemical Impedance Spectroscopy (EIS) tests were carried out at room temperature (22 ± 2 °C) using a frequency response analyser and an electrochemical interface by Solartron. The impedance spectra were obtained in the frequency range between 10 mHz and 10 kHz using a three electrodes arrangement. The three electrodes cell consists of a saturated calomel electrode as reference electrode (placed perpendicularly to the upper side and on a humidified sponge piece to establish contact with the reinforced specimen), a stainless steel plate (placed on the upper side of the specimen) as counter electrode and the galvanized rebar as working electrode (Fig. 1). The working length exposed is 10 cm, the rest of the rebar was masked with epoxy resin. EIS measurements were performed at the open circuit potential (OCP).

3.1.2. Polarization resistance results

Polarization resistance, defined as the diameter of the capacitive arc in the complex plane representation of the impedance obtained at the OCP, was obtained from the EIS spectra at 3, 6 and 12 immersion cycles (Figs. 2 and 3 illustrate, as an example, the Nyquist plot corresponding to the impedance data obtained for S2(DEA,GS) with detailed spectra and fitting are incorporated to the Fig. 3). The results of polarization resistance values obtained are summarized in Fig. 4. It can be noticed that SN addition produces lower polarization resistance values than those corresponding to the

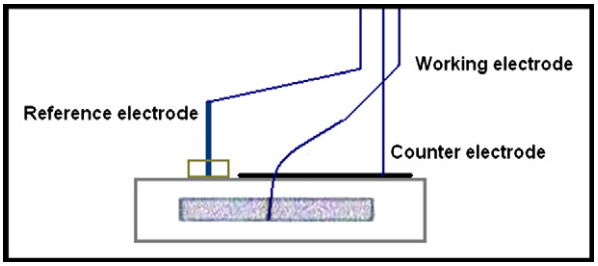

Fig. 1. The three electrodes arrangement used to perform EIS measurements on reinforced specimens.

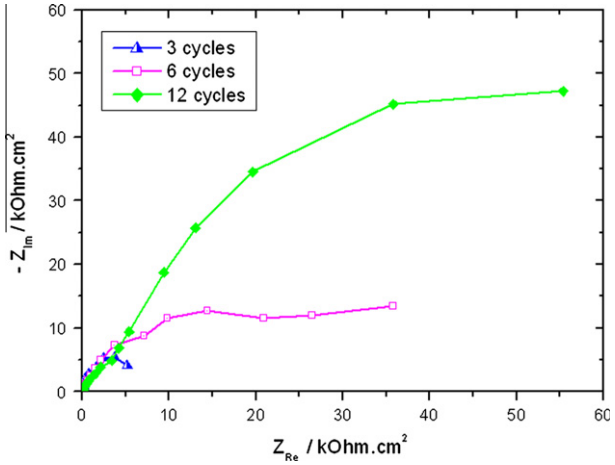

Fig. 2. Nyquist plot corresponding to the impedance data obtained for reinforced mortar specimens with DEA addition (3.5 L/m^3) after 3, 6 and 12 cycles of wet–dry exposure to 3% NaCl solution.

control sample. Moreover, after 12 cycles the R_p values fall below the kΩ scale, which means very high corrosion rate.

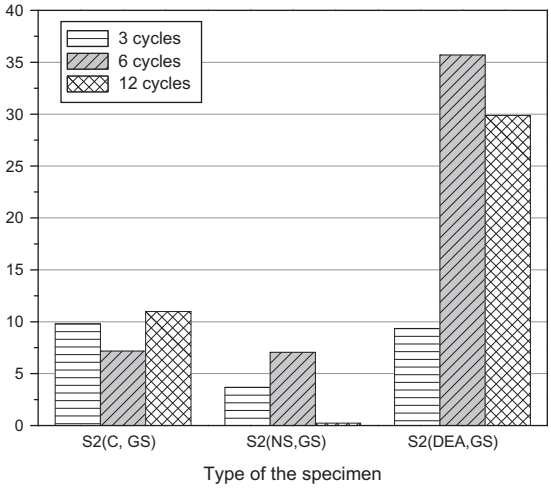

Fig. 4. Evolution of polarization resistance values obtained for reinforced mortar specimens after 3, 6 and 12 cycles of wet–dry exposure to 3% NaCl solution.

On the other hand, the DEA addition increases clearly the polarization resistance value after the 6th cycle of wet–dry exposure.

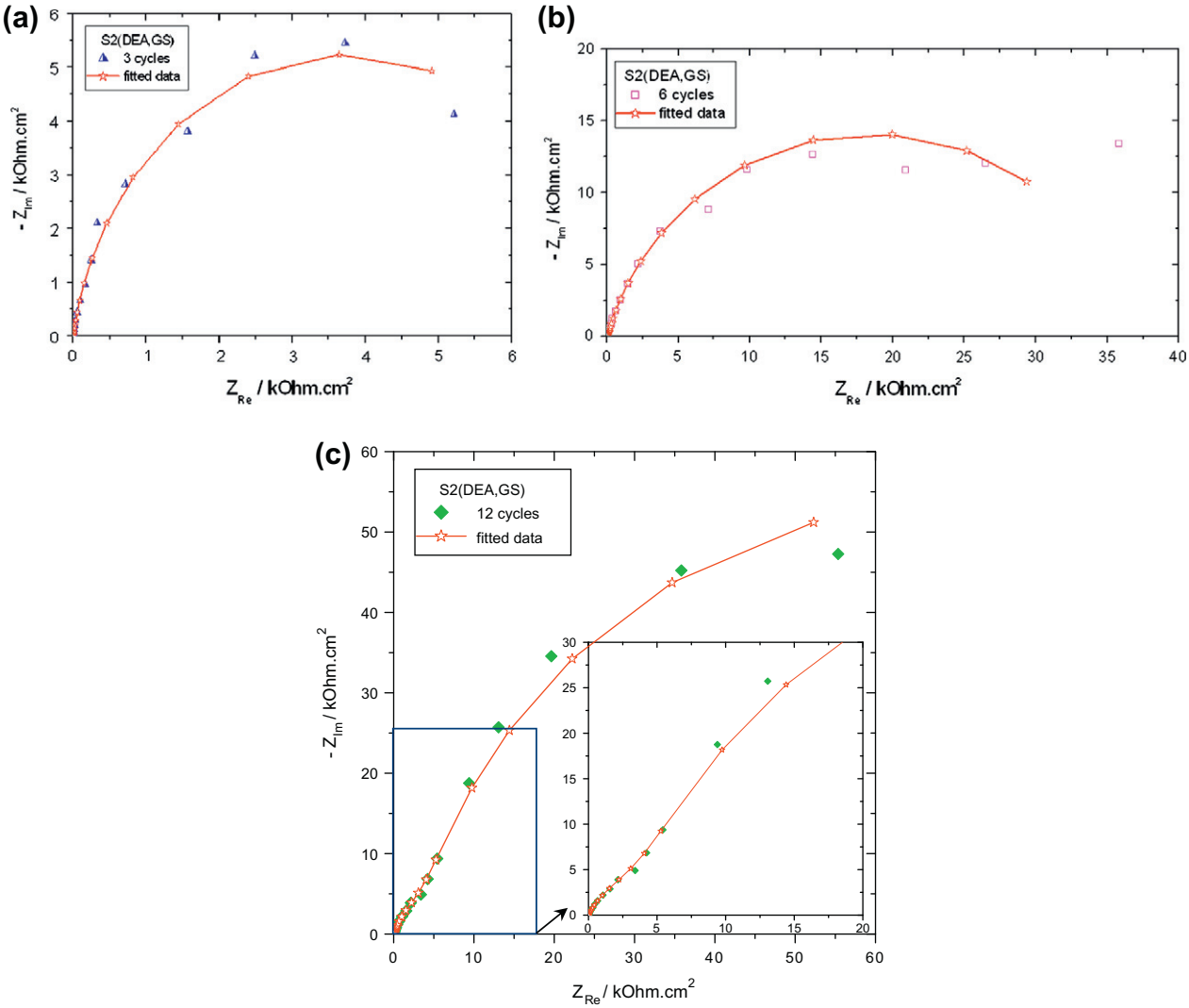

Fig. 3. Nyquist plot corresponding to the impedance data obtained for reinforced mortar specimens with DEA addition (3.5 L/m^3): (a) after three cycles, (b) after six cycles and (c) after 12 cycles of wet–dry exposure to 3% NaCl solution.

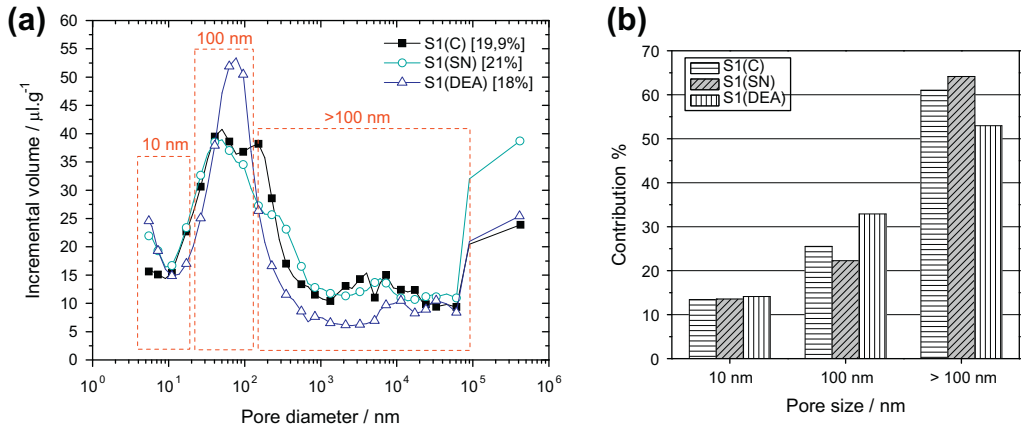

Sample	S1(C)	S1(SN)	S1(DEA)
Total porosity	19.9	21.0	18.0
Family 1 : (> 100 nm)	61.03	64.16	52.97
Family 2 : (100 nm)	25.54	22.27	32.90
Family 3 : (10 nm)	13.43	13.57	14.13

Fig. 5. Mercury Intrusion Porosimetry results corresponding to mortar samples after 28 days curing. (a) Incremental volume of mercury intruded as a function of pore diameter. The total porosity is also indicated in the legend. The three groups of pore families analysed are indicated; (b) relative contribution to total porosity of the three pore families chosen in (a).

Furthermore, in order to validate the obtained results, the mortar specimens were examinated after 12 wet–dry cycles by visual evaluation. This was performed by observing the state of the galvanized bars after splitting the specimens. The galvanized coating, for the specimens S2(C,GS) and S2(SN,GS), was totally dissolved and the state of the reinforcement became similar to an ordinary carbon steel. However, the reinforcement in the specimen S2(DEA,GS) had an aspect similar to that observed for the control specimen but with the presence of some local zones which conserved a galvanized coating. These results revealed the performance of DEA when it is added to mortar to protect galvanized steel reinforcement against corrosion in the case of accelerated corrosion tests. The use of this inhibitor can be quite efficient to protect galvanized steel reinforcements in concrete structures exposed to marine environments.

3.2. Mercury Intrusion Porosimetry (MIP)

3.2.1. Experimental method

MIP was employed for microstructure characterization. This technique enables us to obtain valuable information on pore structure.

The porosimeter utilised was an AUTOPORE IV 9500 from Micromeritics that measures pore diameters from 0.9 mm down to 5 nm thanks to the maximum yield pressure of 227 MPa. In the purpose to make the measuring sample representative of the real pore structure, samples with irregular random shapes were cut from the slices [22].

In the first step of the experiment, there is a stage of air evacuation where the pressure reaches 50 µmHg in the recipient holding the sample in order to evacuate air and moisture in the pores. The second step consists in filling up the recipient with mercury and finally, pressures are applied to the sample. The more the pressure increases, the more the diameter of investigated pore is small. MIP was performed for samples issuing from specimens after curing period and others after the wet–dry exposure to the sodium chloride solution.

3.2.2. Microstructure analysis

The hydration reactions induce the development of interconnected pores of different sizes. The pores can be divided into macropores, capillary pores and gel pores. The capillary pores are the voids not filled by the solid products of hydration. In determining the role of the mortar in protecting the embedded galvanized reinforcements, not only should the total capillary porosity (i.e. the percentage of volume occupied by capillaries) be considered but also the size and the interconnections of capillary pores.

The experimental results of the microstructure analysis are presented in pore size logarithmic scale, as can be seen in Figs. 5a and 6a, which show the pore size distribution and the total porosity obtained for the tested specimens. Figs. 5b and 6b illustrate the relative contribution to total porosity of the three pore families chosen in the purpose to compare the effect of inhibitor addition on mortar microstructure before and after chloride exposure.

MIP performed for samples issuing from specimens after curing period (Fig. 5) reveals that inhibitor addition did not affect the fraction of smallest pores (10 nm); it is about 15% for the three samples. However, an increase of the fraction of larger pores and a decrease of medium size pores were found when SN is used compared to the control sample. But, the addition of DEA seems to decrease the fraction of larger pores (>100 nm) to develop smaller pores, which suggests the formation of a large number of interconnections between larger size pores. This phenomenon will lead to increasing both pore tortuosity and percolation, being responsible to the decreasing of the total porosity for samples with DEA addition.

It can be noticed from MIP results performed on samples issuing from specimens after wet–dry exposure (Fig. 6) that chloride exposure increases the fraction of smallest pores (10 nm), it is about 20% for the three specimens. The microstructure of S2(SN) resembles to the control sample S2(C). However, the exposure to chloride environment of S2(DEA) engenders a small fraction of medium size pores and increases the fraction of larger pores without affecting the total porosity of the sample (15.8% compared to 15% for S2(C)). The decreasing of total porosity for all the samples S2(C), S2(SN) and S2(DEA) is due to the formation of Friedel's salt (the

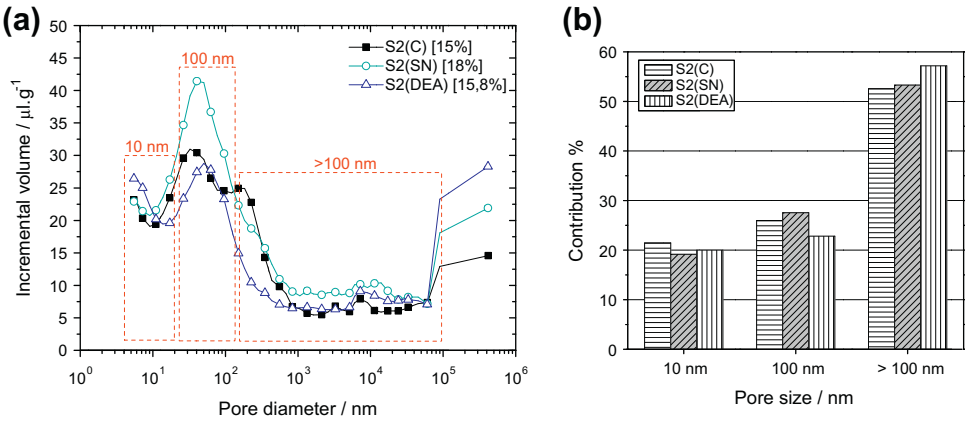

Sample	S2(C)	S2(SN)	S2(DEA)
Total porosity	15.0	18.0	15.8
Family 1 : (> 100 nm)	52.58	53.29	57.17
Family 2 : (100 nm)	25.96	27.55	22.83
Family 3 : (10 nm)	21.46	19.16	20.00

Fig. 6. Mercury Intrusion Porosimetry results corresponding to mortar samples after 28 days curing and seven cycles of wet–dry exposure in a 3% NaCl solution. (a) Incremental volume of mercury intruded as a function of pore diameter. The total porosity is also indicated in the legend. The three groups of pore families analysed are indicated; (b) relative contribution to total porosity of the three pore families chosen in (a).

reaction of cement's C_3A phase and chloride ions) which is a layered structure of calcium aluminates stabilized by chlorides and water, and occupying the interlamellar spaces. EDX and XRD analysis performed on mortar samples saturated with NaCl 1 M solution confirmed this hypothesis [23]. But, the influence of Friedel's salts on the mortar microstructure for specimens containing inhibitors differs from the control sample; the reaction seems to be dependent on the inhibitor addition.

3.3. Impedance Spectroscopy (IS)

3.3.1. Experimental method

3.3.1.1. Mortar permittivity. The IS measurements were performed, from 15 MHz down to 10 kHz, using an HP 4194A impedance gain/phase analyser. Capacitance measurements can be performed in the range of 10^{-14}–0.1 F with a maximum resolution of 10^{-14} F. A non-contacting method, used previously in others studies [22,24,25], was employed by means of the HP 16451B Dielectric Test Fixture (Fig. 7). This method minimizes the possible contribution of the sample–electrode interface. It consists of leaving an air gap between sample and electrode or by placing polyester sheets (100 µm thick) to insulate the electrodes. The impedance of the air gap was measured prior to the samples measurement and numerically subtracted from the overall impedance after measurement, to obtain only the impedance of the sample.

The electrodes employed were high density sheets of graphite. Before testing, samples were left at laboratory atmosphere for natural drying. Then, they were held on vacuum machine to get water evaporation without causing morphological changes. The dielectric constant of the mortar sample is given by the following equation:

$$\varepsilon = \frac{e \times C_1}{\varepsilon_0} \quad (1)$$

where C_1 is the calculated dielectric capacitance (F cm^{-2}), e is the sample thickness (cm) and ε_0 is the vacuum permittivity (8.85×10^{-14} F cm^{-1}).

3.3.1.2. Mortar resistivity. The IS measurements were carried out using the arrangement shown in Fig. 8 connected to the HP

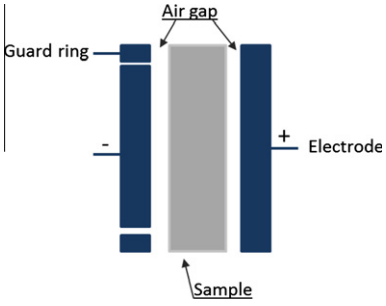

Fig. 7. Flat cell employed for impedance measurements (schematic). Electrodes are circular, ∅ 40 mm.

4194A impedance gain/phase analyser used before in the high frequency range (10 kHz–15 MHz). The sample's resistivity assessment enables us to take into account the diffusion eventuality via percolating capillary porosity. Resistivity is an important parameter assessed in the aim to supply information on the water content in the mortar, the resistance to chloride penetration or the corrosion rate.

Before testing, the mortar samples were pre-conditioned by saturation with NaCl 1 M solution [26]. Samples were kept in the filling solution until performing the measurements.

The resistivity is calculated from the resistance value (R_1) measured between the electrodes (obtained from Nyquist plots) by means of the following equation:

$$\rho = \frac{R_1 \times S}{e} \quad (2)$$

where ρ is the resistivity (Ω m), R_1 is the measured resistance between electrodes (Ω), S is the exposed surface of the mortar sample to the chloride solution (corrected for the electric field dispersion [27]), e is the sample thickness.

3.3.2. Mortar dielectric properties

As it can be seen in Fig. 9, the impedance of the sample is capacitive, so the Cole–Cole transformation (Eq. (3)) is used with the aim

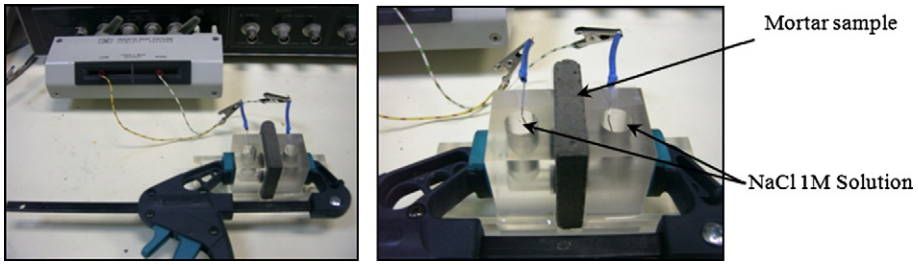

Fig. 8. Arrangement used to determine mortar's resistivity by Impedance Spectroscopy.

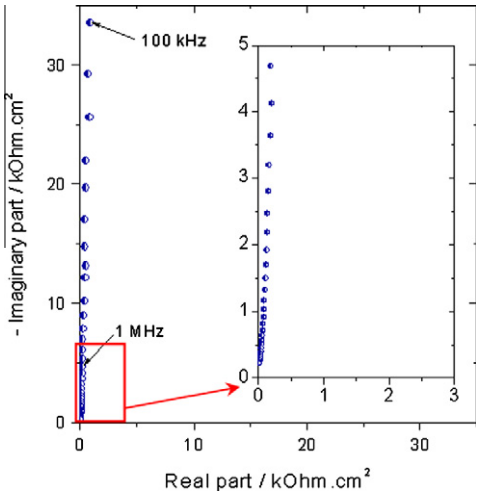

Fig. 9. Nyquist plot corresponding to the impedance data obtained for the control sample after seven cycles of wet–dry exposure to chloride solution.

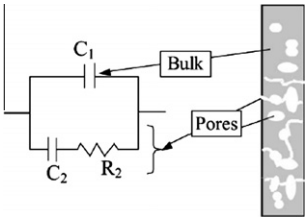

Fig. 10. Schematic representation of the equivalent circuit model employed for fitting high frequency impedance data corresponding to mortar using the non-contacting method. C_1 represents the solid phase contribution, and R_2 and C_2 are attributed to the electrolyte filling the pores [25].

of accurate representations, which have well defined high and low frequency limits. C(ω) is the complex capacitance and Z(ω) the impedance of the sample at angular frequency ω [22].

$$C(\omega) = \frac{1}{j\omega Z(\omega)} \tag{3}$$

The Cole–Cole representation, which is a complex capacitance plot, is considered as the simplest way of studying the dielectric behavior of mortar.

An example of the Cole–Cole transformation of data presented in Fig. 9 is depicted in Fig. 11. The equivalent circuit model employed for fitting impedance data is depicted in Fig. 10. The representation depicted in Fig. 11 corresponds to a typical Cole–Davidson dispersion shape that can be modeled using the following equation [25]:

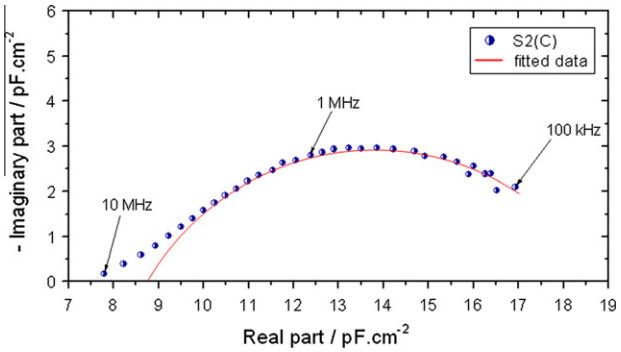

Fig. 11. Cole–Cole plot corresponding to impedance data given in Fig. 7 obtained for the control sample after seven cycles of wet–dry exposure to chloride solution.

Table 3
Summary of Impedance Spectroscopy results for mortar specimens.

		e (cm)	C_1 (pF cm^{-2})	C_2 (pF cm^{-2})	f_m (MHz)	R_2 (kΩ cm^{-2})	ε
Lot no. 1	S1(C)	0.89	7.9	14.1	0.88	1284.7	7.9
	S1(SN)	0.86	8.0	10.0	1.91	833.7	7.8
	S1(DEA)	0.88	8.5	11.6	1.63	842.2	8.5
Lot no. 2	S2(C)	0.89	8.8	18.9	0.52	1604.8	8.9
	S2(SN)	0.85	7.5	12.0	0.90	1461.4	7.2
	S2(DEA)	0.87	8.4	12.3	1.17	1106.5	8.3

$$C(\omega) = C_1 + \frac{C_2}{(1 + (j\omega R_2 C_2)^{\alpha})^{\beta}} \tag{4}$$

where the α and β parameters are constants, $0 < \alpha$, $\beta \leqslant 1$, that account respectively for the symmetric (Cole–Cole) and asymmetric (Cole–Davidson) dispersion of the R_2C_2 time constant.

The high frequency limit of the Cole–Cole plot, C_1, is defined by the dielectric capacitance of the solid phase in the mortar while the capacitance, C_2, defines the low frequency limit of the complex capacitance plot ($C_1 + C_2$) and it is directly linked to the double layer capacitance formed at the C–S–H gel layers limiting occupied pores. C_2 and the resistance R_2 are parameters associated to the contribution of the liquid phase filling pores. Subsequently, these parameters have both a strong dependence on the amount of water in the sample as well as on pore structure [22].

The obtained dielectric parameters C_1, C_2 and R_2 are depicted in Table 3. The capacitance C_1, obtained from the plot, enables us to calculate the apparent dielectric constant of the mortar sample [28], which is proportional to the fraction of solid phase present in the system (compactness degree).

The data reported in Table 3 are in good agreement with the MIP results. For the cured samples (Fig. 3, lot no. 1 in Table 3) it can be seen that samples with DEA addition present the lower

porosity (18%) and also higher apparent dielectric constant (compactness). Changes in the porosity distribution are related to the R_2C_2 time constant, which decreases in presence of the inhibitors (the characteristic frequency increases). Moreover, the decreased R_2 values for the mixes containing the inhibitors suggest an increased conductivity of the pore electrolyte.

For the lot no. 2, the lowest apparent dielectric constant corresponds to the samples with SN addition, in accordance with the total porosity value reported in Fig. 6 were those samples show the highest porosity. The effect of the Friedel's salt precipitation is evident in the R_2C_2 time constant: R_2 increases with respect to the unexposed samples, and C_2 increases too due to increased tortuosity of the pore network.

3.3.3. Mortar resistivity

The equivalent circuit in this case is depicted in Fig. 12. The only difference with the one used in the previous section (Fig. 10) is the additional parameter, R_1, which accounts for sample's resistivity i.e., resistance associated to percolating pores [23,25]. So, the resistivity is related to the conductivity of the solution filling pores (resistivity increases as the ionic concentration of this solution decreases). Fig. 13 corresponds to the normalized impedance corresponding to the mortar sample S2(SN). R_1 corresponds to the diameter of the high frequency capacitive arc in Fig. 13. The low frequency contribution (below 1 MHz) corresponds to the electrodes.

As expected (see Table 4), the mortar resistivity correlates well with the conductivity of the solution filling pores: resistivity value increases when mortar sample is submitted to wet–dry cyclic test. Thus, it can be said that during the wetting period chloride ions penetrate in capillary pores and form Friedel's salt which clinged to the pore surface during the drying period. The resistivity increases with the hydration of the cement. A decrease of the resistivity value explains an increase of the amount of water-filled pores. An increased resistivity is accompanied by a reduced corrosion rate [22].

The increasing of the mortar resistivity in presence of DEA reveals the performance of this inhibitor to improve the hydration process of the mortar. Indeed, this result can be explained by the decreasing of the amount of water filling pores. It is well known that a high resistivity value means a better corrosion resistance of the material because of the improved barrier properties. Thus, DEA can be considered as a good corrosion inhibitor for steel reinforcements with respect to the control sample. However, results obtained in the presence of SN clearly show the inefficiency to protect reinforcements when they are embedded in mortar.

3.4. Differential Scanning Calorimetry (DSC)

3.4.1. Experimental method

Thermal analysis has proved to be a valuable technique in the study of cement hydration [29,30]. DSC is considered as an important tool for evaluating the nature of hydrated products.

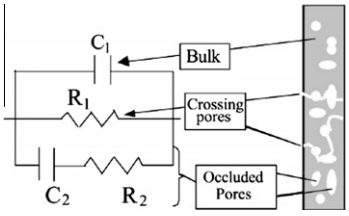

Fig. 12. Schematic representation of the equivalent circuit employed to model the data corresponding to saturated mortar samples with NaCl 1 M solution [25].

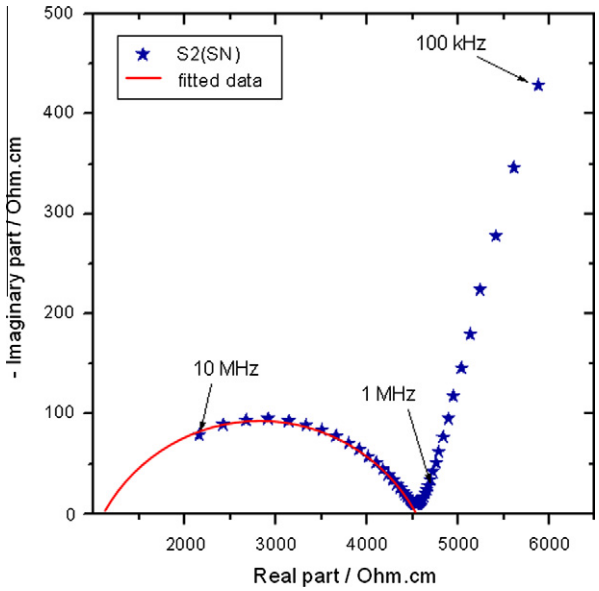

Fig. 13. Normalized impedance spectrum (Nyquist plot) corresponding to the mortar sample with 2% sodium nitrite addition after seven cycles of wet–dry exposure to chloride solution used to obtain the mortar resistivity.

Table 4
Mortar resistivity values.

	Specimen	e (cm)	R_1 (Ω)	ρ (Ω cm)
Lot no. 1	S1(C)	0.87	2250	2030
	S1(SN)	0.89	2100	1852
	S1(DEA)	0.86	3508	3202
Lot no. 2	S2(C)	0.87	3760	3392
	S2(NS)	0.86	3214	2934
	S2(DEA)	0.87	4500	4060

The DSC tests were performed on specimens of lot no. 1 using an 822 Mettler Toledo calorimeter with a computer-controlled furnace. The samples were heated in the range 25 up to 700 °C at a constant rate (10 °C/mn) in a dynamic nitrogen atmosphere (20 ml/mn). This method of thermal analysis was applied to investigate the effect of inhibitor addition on the process of cement hydration and to identify the formation of dehydrated and transformed phases of mortar samples. The analysis was performed on mortar samples taken from portions in the middle of the mortar slices. DSC curves of mortar specimens are shown in Fig. 14. The samples used weighted around 30 mg.

3.4.2. DSC results

Fig. 14 shows the DSC curves obtained for mortar samples after 28 days. These curves are plotted with the endothermal behavior in the downward direction, as is the convention in most of the cement and concrete literature. A number of peaks were observed and these curves can be divided into five major parts, according to different reactions:

- 25–115 °C: dehydration of pore water.
- 115–420 °C: different stages of C–S–H dehydration.
- 420–480 °C: dehydroxylation of $Ca(OH)_2$.
- 480–600 °C: conversion of SiO_2.
- 480–700 °C: decarbonation of $CaCO_3$.

From 25 to 200 °C, the free water and a part of the bound water of hydrated products escape such as C–S–H gel [31] and the

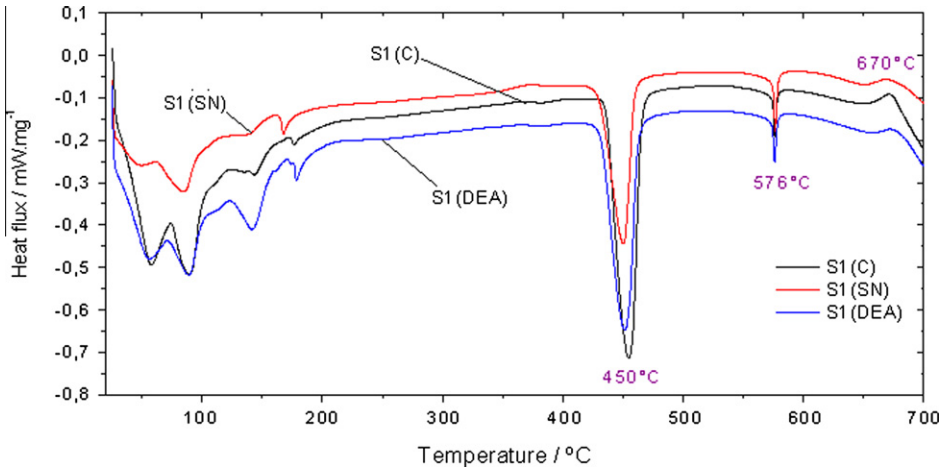

Fig. 14. Differential Scanning Calorimetry curves of mortar samples after 28 days of curing.

decomposition of ettringite takes place [32]. Indeed, the peak before 100 °C corresponds to the C–S–H gel dehydration.

The C–S–H peak, occurring at around 140 °C, is increased with the use of DEA. The peak observed at 175 °C corresponds to the ettringite, resulting from the reaction between C_3A and gypsum (gypsum is added in ordinary Portland cement to avoid the fast hydration of C_3A).

Up to 400 °C, the bound water is lost in C–S–H gel, which is transformed into a modified C–S–H and partially dehydrated C–S–H with low crystalline structure [31,33].

At 576 °C, the peak is similar for all mortar samples; it is due to the conversion of quartz (SiO_2) in the sand [34]. This effect can cause a volume expansion and make the sand broken.

All curves show an exothermic peak in the vicinity of 450 °C, it corresponds to the dehydroxylation of portlandite (decomposition of $Ca(OH)_2$ to CaO and H_2O), another hydration product [33], but this peak is less intense for mortar sample containing SN indicating less Ca(OH)2 content. It is known that SN is slight acid and can neutralize calcium hydroxide. X-ray analysis confirmed the absence of $Ca(OH)_2$ in DSC samples heated to 635 °C. And the peak at 670 °C corresponds to the decarbonation of calcium carbonate [29].

Continuously heating to 700 °C, the decarbonation of calcium carbonate and the complete dehydroxylation of calcium hydroxide occur [34,35]. In addition, the C–S–H gel completely changes into dehydrated C–S–H [33].

4. Discussion

The results presented above reveal the effect of the DEA as a corrosion inhibitor for steel in concrete is twofold: direct and indirect. The direct action concerns the faradaic process that is hindered in presence of the amine, as the polarization results reveal. The indirect action concerns the barrier-forming effect because it decreases the porosity of the concrete and increases resistivity.

Dielectric properties clearly reflect the pore structure development and the degree of pore occupancy by electrolyte.

MIP results show also that the microstructure of mortar evolves in presence of chlorides, mainly due to the formation of Friedel's salts. Overall porosity changes, new pore families develop and pore's tortuosity too.

The variations in R_2 values are closely related to the hydration process of the mortar. The hydration involves the reaction of $C_3S(3CaOSiO_2)$ and $C_2S(2CaOSiO_2)$ with free water to form calcium silicate hydrate (C–S–H) and calcium hydroxide [36]. These reactions promote the formation of a rigid microstructure and strength development.

It can be also noticed the existence of a clear dependence between permittivity values and the samples porosity. The permittivity evolution mimics the evolution of the total porosity: the sample's permittivity increases as the porosity decreases. In a previous study [28] on cement paste hardening process, researchers obtained a linear dependence of permittivity with w:c ratio. As for given cement paste the w:c ratio determines its porosity, permittivity measurements can provide a fast method of real time evaluation of the sample's porosity.

The porosity increasing decreases the volume fraction of solid phase and hence the associated capacitance values decrease too.

DEA seems to react with hydration products. The reaction with $Ca(OH)_2$ results in a gel formation that block the pores of the mortar. The pore-blocking effect is a secondary property as it causes a reduction in the chloride ingress into mortar. Subsequently, the corrosion process is delayed.

Another interesting feature concerns the inhibitors effect on the hydration process of mortar samples. From the Calorimetry investigations performed, showed in the DSC curves, it is possible to conclude that inhibitors did not influence generally the cement hydration, but, it is clearly shown that there is a modification in the stages of C–S–H dehydration especially with the addition of DEA.

It's also clear that the addition of SN modified the dehydroxylation of portlandite process (decomposition of $Ca(OH)_2$ to CaO and H_2O) shown in the peak in the vicinity of 450 °C. This is owing to the acidity of SN which causes the neutralization of calcium hydroxide i.e. less $Ca(OH)_2$ content. This influence corroborate the results obtained for the total porosity (21%) of the specimens S1(SN) which can explain the negative effect when specimens were exposed to chloride environment. However, the use of DEA did the opposite effect on the dehydroxylation of portlandite process which can explain less porosity (18%) and then a good performance in presence of chlorides with respect to the control specimens.

5. Conclusions

The above-discussed results reveal interesting aspects of using galvanized coating and inhibitor addition. In particular, these two preventive methods act in a complementary manner to delay corrosion: galvanizing protects the steel reinforcement and the inhibitor reacts with mortar by improving its performance in presence of chloride environment.

The evolution of polarization resistance values, measured on reinforced mortar specimens after 3, 6 and 12 cycles of wet–dry exposure to 3% NaCl solution, show that the corrosion resistance

of galvanized rebars is improved in presence of DEA with respect to the control specimen, contrary to the use of SN which accelerates the corrosion process.

Impedance measurements in the frequency range (10 kHz–15 MHz) can supply information on pore network development as well as on pore occupancy; these measurements, with Mercury Intrusion Porosimetry results corresponding to mortar samples after 28 days curing, showed that the inhibitor addition influenced the microstructure and the pore distribution of the mortar (a decrease of the total porosity with the DEA and an increase of total porosity with the SN). These changes were explained by the effect of the inhibitor on the components of the mortar, especially the effect on the dehydroxylation of portlandite process shown by the DSC results.

The above discussed results show also that the microstructure of mortar evolves in presence of chlorides (mainly due to the formation of Friedel's salts). Overall porosity changes, new pore families develop and pore system tortuosity also changes. There exists a clear dependence between permittivity values and sample porosity. The permittivity evolution mimics the evolution of the total porosity: the sample's permittivity increases as the porosity decreases.

The results obtained in this work clearly show that the corrosion behavior of galvanized steel in reinforced mortar specimens is greatly improved by the addition of DEA, which acted as an efficient corrosion inhibitor in chloride environment by influencing the microstructure of the mortar.

References

[1] Macias A, Andrade C. The behaviour of galvanized steel in chloride-containing alkaline-solutions. I: The influence of the cation. Corros Sci 1990;30(4–5):393–407.

[2] Yeomans SR. Performance of black, galvanized and epoxy-coated reinforcing steels in chloride-contaminated concrete. Corrosion 1994;50(1):72–81.

[3] Bautista A, Gonzalez JA. Analysis of the protective efficiency of galvanizing against corrosion of reinforcements embedded in chloride contaminated concrete. Cem Concr Res 1996;26(2):215–24.

[4] Ramirez E, Gonzalez JA, Bautista A. The protective efficiency of galvanizing against corrosion of steel in mortar and in $Ca(OH)_2$ saturated solutions containing chlorides. Cem Concr Res 1996;26:1525–39.

[5] Belaid F, Arliguie G, François R. Corrosion products of galvanised rebars embedded in chloride-contaminated concrete. J Sci Eng Corros 2000;56(9):960–5.

[6] Yeomans SR, editor. Galvanized steel reinforcement in concrete. Elsevier; 2004.

[7] Darwin D, Browning J, O'Reilly M, Xing L, Ji J. Critical chloride corrosion threshold of galvanized reinforcing bars. ACI Mater J 2009;106(2):176–83.

[8] Ghosh R, Singh DDN. Kinetics, mechanism and characterization of passive film formed on hot dip galvanized coating exposed in simulated concrete pore solution. Surf Coat Technol 2007;201(16–17):7346–59.

[9] Okamura H, Hisamatsu Y. Effect of use of galvanized steel on the durability of reinforced concrete. Mater Perform 1976;15(7):43–7.

[10] Fratesi R, Moriconi G, Coppola I. The influence of steel galvanization on rebars behaviour in concrete. In: Page CL, Bamforth PB, Figg JW, editors. Corrosion of Reinforcement in Concrete Construction. Royal Society of Chemistry; 1996. p. 630–41.

[11] Swamy RN. Resistance to chlorides of galvanized rebars. In: Page C, Treadaway KWJ, Bamforth PB, editors. Corrosion of Reinforcement in Concrete. London, New York: Elsevier Appl. Sci; 1990. p. 586–600.

[12] Fratesi R. Galvanized reinforcing steel bars in concrete. COST 521 workshop, Luxembourg; 2002.

[13] Comité Euro-International de Béton (CEB). Protection systems for reinforcement. Bulletin d'information No. 211, 1992, Paris.

[14] Montemor MF, Simões AM, Ferreira MGS. Composition and corrosion behaviour of galvanised steel treated with rare-earth salts: the effect of the cation. Prog Org Coat 2002;44(2):111–20.

[15] Ferreira MGS, Duarte RG, Montemor MF, Simões AMP. Silanes and rare earth salts as chromate replacers for pre-treatments on galvanised steel. Electrochim Acta 2004;49(17–18):2927–35.

[16] Trabelsi W, Cecilio P, Ferreira MGS, Montemor MF. Electrochemical assessment of the self-healing properties of Ce-doped silane solutions for the pre-treatment of galvanised steel substrates. Prog Org Coat 2005;54(4):276–84.

[17] Sánchez M, Alonso MC, Cecílio P, Montemor MF, Andrade C. Electrochemical and analytical assessment of galvanized steel reinforcement pre-treated with Ce and La salts under alkaline media. Cem Concr Compos 2006;28(3):256–66.

[18] Jamil HE, Shriri A, Boulif R, Bastos C, Montemor MF, Ferreira MGS. Electrochemical behaviour of amino-alcohol-based inhibitors used to control corrosion of reinforcing steel. Electrochim Acta 2004;49(17–18):2753–60.

[19] Buffenbarger JK, Miltenberger MA, Miller BD, Casal HL. Long term performance of organic inhibitors. In: Proceedings of the international congress on advanced materials, their process and applications, Munich, September 2000.

[20] Brown MC, Weyers RE, Sprinkel MM. Effect of corrosion-inhibiting admixtures on material properties of concrete. ACI Mater J 2001;98(3):240–50.

[21] De Schutter G, Luo L. Effect of corrosion inhibiting admixtures on concrete properties. Constr Build Mater 2004;18(7):483–9.

[22] Cabeza M, Keddam M, Nóvoa XR, Sánchez I, Takenouti H. Impedance spectroscopy to characterize the pore structure during the hardening process of Portland cement paste. Electrochim Acta 2006;51(8–9):1831–41.

[23] Díaz B, Freire L, Merino P, Nóvoa XR, Pérez MC. Impedance spectroscopy study of saturated mortar samples. Electrochim Acta 2008;53(25):7549–55.

[24] Keddam M, Takenouti H, Nóvoa XR, Andrade C, Alonso C. Impedance measurements on cement paste. Cem Concr Res 1997;27(8):1191–201.

[25] Cabeza M, Merino P, Miranda A, Nóvoa XR, Sanchez I. Impedance spectroscopy study of hardened Portland cement paste. Cem Concr Res 2002;32(6):881–91.

[26] ASTM Standard C 1202-97. Standard test method for electrical indication of concrete's ability to resist chloride ion penetration, Annual Book of ASTM Standard, Section 4, vol. 04.02, 2000.

[27] Díaz B, Freire L, Nóvoa XR, Puga B, Vivier V. Resistivity of cementitious materials measured in diaphragm migration cells: the effect of the experimental set-up. Cem Concr Res 2010;40(10):1465–70.

[28] Andrade C, Blanco VM, Collazo A, Keddam M, Nóvoa XR, Takenouti H. Cement paste hardening process studied by impedance spectroscopy. Electrochim Acta 1999;44(24):4313–8.

[29] Bhatty JI. A review of the application of thermal analysis to cement–admixture systems. Thermochim Acta 1991;189(2):313–50.

[30] Abdelrazig BEI, Main SD, Nowell DV. Hydration studies of modified OPC pastes by differential scanning calorimetry and thermogravimetry. J Therm Anal 1992;38(3):495–504.

[31] Alarcon-Ruiz L, Platret G, Massieu E, Ehrlacher A. The use of thermal analysis in assessing the effect of temperature on a cement paste. Cem Concr Res 2005;35(3):609–13.

[32] Castellote M, Alonso C, Andrade C, Turrillas X, Campo J. Composition and microstructural changes of cement pastes upon heating, as studied by neutron diffraction. Cem Concr Res 2004;34(9):1633–44.

[33] Alonso C, Fernandez L. Dehydration and rehydration processes of cement paste exposed to high temperature environments. J Mater Sci 2004;39(9):3015–24.

[34] Grattan-Bellew PE. Microstructural investigation of deteriorated Portland cement concretes. Constr Build Mater 1996;10(1):3–16.

[35] Handoo SK, Agarwal S, Agarwal SK. Physicochemical, mineralogical, and morphological characteristics of concrete exposed to elevated temperatures. Cem Concr Res 2002;32(7):1009–18.

[36] Taylor HFW. Hydration of the calcium silicate phases, cement chemistry. 2nd ed. London: Thomas Telford Publishers; 1998. p. 113 [chapter 5].